ARCHAEOMETALLURGICAL EVALUATION OF FINERY USING NONDESTRUCTIVE METHODS

I. FIERASCU[1], R.C. FIERASCU[1*], D.A. MIREA[2], P. FOTEA[1,3], R.F. ANDREI[2], A. ORTAN[4]

[1] National Institute for Research & Development in Chemistry and Petrochemistry – ICECHIM Bucharest, 202 Spl. Independentei, 060021 Bucharest, Romania
[2] "Horia Hulubei" National Institute for Nuclear Physics and Engineering, 30 Reactorului Str., 077125 Magurele, Ilfov, Romania
[3] Romanian Peasant Museum, 3 Kiseleff Ave., 011341, Bucharest, Romania
[4] University of Agronomic Sciences and Veterinary Medicine of Bucharest, 59 Marasti Blvd., 011464 Bucharest, Romania
*Corresponding author: *radu_claudiu_fierascu@yahoo.com*

Abstract. Throughout the history, the ornaments made to be worn accompanied the human development, representing an important source of information regarding various cultures' habits and technology. As those objects are made from durable materials, we now can evaluate the techniques and materials used to create them. The study of such objects, even though can provide invaluable information, should meet some critical criteria, one of the most important being the non-destructive character of the techniques used. The objects selected for the study represents jewelry from late XIXth century – early XXth century (one yellow-color pendant, manufactured at the end of the XIXth century, one medallion manufactured at the beginning of the XXth century and two roman coins, from the Augustus period and, respectively, republican age, modified and turned into a bracelet part, respectively into a brooch). The objects were studied using exclusively non-destructive techniques: optical microscopy, X-ray fluorescence, X-ray diffraction and Particle-induced X-ray emission, the results leading to conclusions regarding not only the composition of the materials and the presence of corrosion compounds, but also regarding the applicability of different techniques for the study of metallic artifacts. The results revealed some "hidden" characteristics of the samples: two of the samples are plated objects (gilded silver, respectively silver-plated brass), while the other two objects were modified using different alloys than the original pieces.

Key words: cultural heritage artifacts, nuclear techniques, analytical characterization.

1. INTRODUCTION

Ever since antiquity, continuing with the Middle Ages, the modern and contemporary era, silver and gold had both material and spiritual significance. The diversity of the objects made from precious materials is vast, as well as religious objects and as civil ones, and over time had a spectacular development and

evolution. Silver has always been considered precious, a purifying and disinfecting metal; gold was the first and most stable material for creating precious objects or gilded surfaces [1]. The term "jewelry" includes articles made from raw materials as noble metals, gemstones, etc. The term "adornment" includes articles made of cheap and synthetic raw materials, imitation of stones, ceramics and in modern times, plastics.

The oldest known pieces of jewelry were discovered in the Siberian region Altai, dating to the Denisovan occupation [2]. The coin is the invention of the ancient Greeks and originally appeared as an intrinsic value piece for the trade. The first coins issued for this purpose were engraved only with symbols, distinctive signs of fortresses or kingdoms. Subsequently, the engravings of the Hellenic protector gods, such as Athens, Helios, Zeus, Apollo, Heracles, Dionysos, began to appear on coins, followed by inscriptions and effigies of the kings. The reason that the first inscriptions and the first effigies appeared on the issued coins was the need for communication between the ruling elite, the leaders, the population of a country or an empire.

Silver and gold are suitable for all types of jewelry, which are distinguished by fashion and working technique, some are polychrome with a bright effect and harmonious shapes. Their alloy, called *electrum*, is extensively encountered in the ancient finery; its color was defined by the silver content, having different shades of yellow [3–5]. Starting with the XIVth century the most used silver is silver 925, which is an alloy of 92.5% pure silver and 7.5% copper. The jewelry manufacturing processes are the same for the two metals. There is a growing demand for so-called white silver or *sterling silver*, which imitates white gold, gives those interested an ornament similar to a gold, but at an obvious lower price. Silver that is not described as Sterling or 92.5 / 925 / .925 has a lower silver content and will often be darker and less bright [1, 6]. The jewelry produced in the XIXth century is characterized by a stylistic eclecticism that takes its inspiration from all past styles; it shows reminiscent of Byzantine and Islamic art and the increasing connection with Constantinople and the Occident left a complex footprint in terms of ornamentation: realistically designed vegetal motifs, heraldic medallions. In the XIXth century and early XXth, the establishment of large artistic commercial firms that produced high-quality jewelry suited to the requirements of the prosperous new bourgeois class led to the manufacture of jewelry which are famous nowadays, like Fabergé, Cartier or Tiffany.

The objects selected for the study represent jewelry from the early XXth century. While objects A and B represent jewelry forged in the XXth century, objects C and D have a very different history. The objects themselves represent Roman coins (sample D having a high numismatic value) transformed into ornaments: sample C was part of a bracelet, being added a silver ring on the reverse and other joints; sample D was transformed into a brooch by adding a silver needle on the

reverse. As the objects studied originated from a private collection, the storage conditions were not special, like those one from the museums. Thus, the objects can present corrosion products, whose study can provide "example information" useful for conservatives and restorers, products which can appear due to atmospheric conditions [7, 8]. The objects were studied using exclusively non-destructive techniques: optical microscopy, X-ray fluorescence, X-ray diffraction and Particle-induced X-ray emission. The integrated protocol established allows the obtaining of information from different complementary techniques (such as those used in our study), with proven application in investigating the microchemical structure of objects and the metallurgical features preserved on their surfaces [9–12]. Also, a combined approach of history/art history research and analytical techniques can be very useful for deciphering the manufacturing techniques and providing information that can later be used for other researchers or conservationists / restorers [1].

2. MATERIALS AND METHODS

2.1. ANALYZED FINERY

The object analyzed in study are presented in Fig. 1.

Fig. 1 – Finery analyzed in the study.

Sample A – Pendant; the object is of yellow color, manufactured at the end of the nineteenth-century, in orthodox rite, with a diameter 30 mm, weight 4.8018 g. The decor is simple and only on the obverse. In the middle is represented *Christ Pantocrator*, and above the head is a bow. Between the two decors there is a circular decor cut off with a tear-like finish, and inside three, four and four more points, repetitive on the left and right. On the right and left side of the human image there is a Cyrillic inscription with *Christ Pantocrator*. In the middle of the bow is caught a ring for the chain (Fig. 1a). Due to its color, the object is probably made out of gold, gold alloy or gilded silver.

Sample B – Medallion; the object is manufactured at the beginning of the XXth century, catholic rite. The medallion is circular and ovalized, diameter 21 mm/9 mm, weight 1.3338 g. The decor is simple: in the middle is represented the Mother of God with the Child in her arms. On the edges there is a circular decoration (Fig. 1b); good condition of preservation, functional wear.

Sample C – Roman coin (*denar*) transformed into a piece of bracelet. The object is made of silver, in the IIIrd century BC (Augustus period) with a diameter of 19 mm, weight 3.6955 g. On the obverse is the effigy of Emperor Augustus, the head laureate to the right with a pearled contour, and the inscription can be translated as *Emperor Nerva Traian Augustus, the Conqueror of Germany*. On the reverse is a zoomorphic humanoid figure with a prey in his right hand. The image is very blunt. The coin has been turned into a jewelry item (bracelet). Production technology: die-casting with two valves, polishing. Conservation state: very worn, turned into a bracelet by adding a disc on the reverse, all around the coin, and by it welded and attached by two pins each, four small rings: two on the left, two on the right (Figure 1c).

Sample D – Roman coin; made of silver in the republican age, with a diameter about 17 mm, weight 3.7179 g. On the obverse is represented Caesar the Emperor, made by casting in the negative. On the reverse is a standing warrior with the spear on the shoulder, and on the right a shield, while on the left is represented an A. Everything is framed in a pearl circle. Deciphering on the reverse cannot be done because, in addition to being bent, it is fragmented on the written part. Production technology: casting, polishing. Moderate state of preservation with corrosion products. Very worn-out, especially on the reverse and on the edge.

2.2. ANALYSIS METHODS

The objects were studied using exclusively non-destructive techniques: optical microscopy, X-ray fluorescence, X-ray diffraction and Particle-induced X-ray emission.

The preliminary evaluation of the coins was performed using an OPTIKA B-150DBR microscope, at different magnifications, in order to observe not only their characteristic features, but also the corrosion layer present on the samples [9].

For the X-ray Fluorescence measurement were used an energy-dispersive spectrometer PW4025, type MiniPal 2 (PANalytical, B.V., The Netherlands), with a Si-PIN detector, at 20 kV and automatic current intensity, measurement time 300 seconds, in Helium atmosphere (beam spot area 81.7 mm^2) [14] for *bulk* analysis and a portable XRF spectrometer Olympus VANTA C (equipped with a 40 kV X-ray tube rhodium anode, Silicon Drift Detector) using the collimated beam option (3 mm) for the *micro-area* analyses; the *micro-area* determinations were performed in four points randomly selected on the surface of the samples. X-ray fluorescence instruments (either portable or benchtop version) are proven to be important tools for the investigation of a wide range of historical artifacts [10, 11, 15, 16].

X-ray diffraction analyses were performed using a Rigaku SmartLab equipment, operating at 45 kV and 200 mA, using $Cu_{K\alpha}$ radiation (1.54059 Å), in parallel beam configuration (2θ/θ scan mode) for *bulk* analyses and in *point focus* configuration with *CBO-f* optics for *micro-area* determinations, as previously presented [9], the *micro-area* analyses being performed in four points randomly selected on the surface of the samples; the components were identified using the Rigaku Data Analysis Software PDXL 2, database provided by ICDD.

The 3MV Tandetron^{TM} particle accelerator installed at the "Horia Hulubei" National Institute for R&D in Physics and Nuclear Engineering (IFIN-HH) [17] was used to generate and deliver a proton beam onto the samples, thus applying the Particle Induced X-ray Emission (PIXE) analysis technique. The samples were irradiated in high vacuum conditions, 10^{-6} atm approximately, using the IBA vacuum chamber installed.

A proton beam of 3 MeV was generated and directed towards the samples. The resulting characteristic X-ray spectra were recorded using a Silicon Drift Detector (SDD, Amptek, USA) set backwards with respect to the proton beam at 45° and analyzed using the Gupix software [18]. PIXE was selected as an appropriate method for the study, due to its proven ability to provide accurate results when historical artifacts [19, 20].

3. RESULTS AND DISCUSSION

The preliminary assessment of the analyzed samples, realized by optical microscopy was aimed to identify the possible corrosion points and other surface features present. The images are presented in Fig. 2.

The surface features presented in Fig. 2 reveal the relatively good state of preservation of samples A and B (with very few corrosion points), as well as the abundance of corrosion products present on samples C and D. All the samples

present scratches on their surface, normal due to their age and destination as finery objects. Sample A presents some corrosion points that could be an indicator of a gilded silver. The most probable corrosion products that could appear on the surface of silver/copper objects are chlorargyrite and tenorite (with a black color), cuprite (reddish brown color), paratacamite or malachite (green color) [9, 21, 22]. For samples C and D are visible the points were supplementary decorations were added to the original coins (the pin and ring on Sample C – Figs. 2C1 and 2C2, respectively the splice area on sample D – Fig. 2D3).
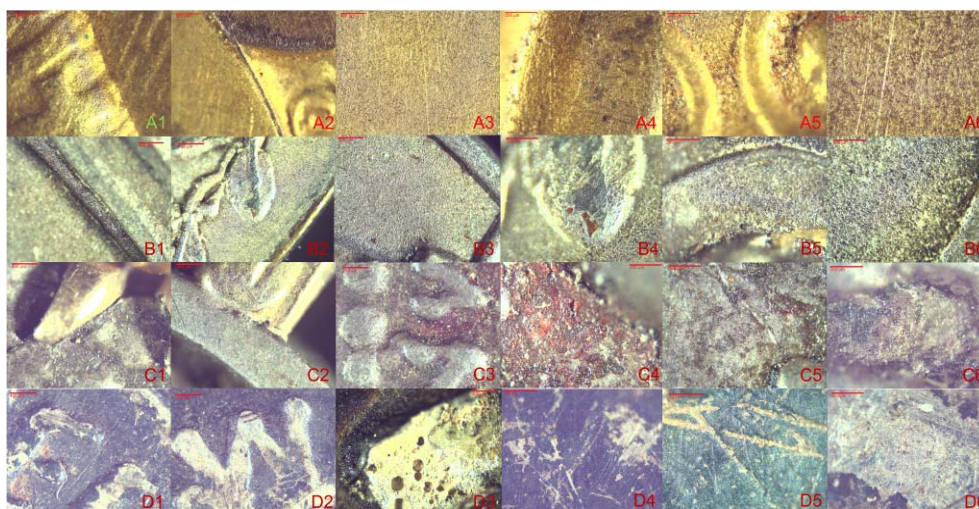

Fig. 2 – Surface features of the samples, observed by optical microscopy
(A to D – sample encoding, scale on image: 1 to 3–400 µm, 4 to 6–200 µm) (Color online).

The analyses performed by *bulk* XRF should provide a clearer image regarding their composition. The XRF spectra are presented in Fig. 3, while the corresponding results are presented in Table 1.

Besides the elements presented in Table 1, other trace and minor elements are present in the samples: Si and Cr in *Sample A*, Si in *Sample B*, Si, Cl, Cr and Pb in *Sample C*, P and Pb in *Sample D*. The presence of minor elements can usually be explained by their presence in the ores used for manufacturing or as a result of contamination during manufacturing processes [9].

Correlated with the XRF results, the *bulk* XRD analysis (Fig. 4) can elucidate the major composition of the samples, as well as it can indicate the major corrosion products present on the surface.

The diffractograms are dominated by the peaks associated with the diffraction planes of a silver-copper alloy (ICDD PDF Card No. 04-010-7444): thus, the peaks numbered in Fig. 4 as 9, 12, 20, 22 and 23, present at 38.17, 44.20, 64.36,

77.41 and, respectively, 81.71 (2θ degrees) correspond to (111), (200), (220), (311) and, respectively, (222) diffraction planes of the alloy. Those diffraction planes are also present in the diffractogram of *Sample A*, but it must be remembered that the peaks could overlap those specific to gold: 38.27 – (111), 44.60 – (200), 64.68 – (220), 77.55 – (311) – ICDD PDF Card No. 00-001-1172. Also, in the diffractogram of *Sample A* appears a peak specific to gold (peak no. 24, at 82.35 degrees – plane (222)). Peaks nos. 10 (40.7 degrees) and 25 (87.9 degrees) correspond to diffraction planes (110) and (220) of a Silver Zinc alloy (ICDD PDF Card No. 00-029-1155), while peak no. 14 (47.2 degrees) could be attributed to the (102) diffraction plane of Zincite (ICDD PDF Card No. 00-036-1451), but without a definitive assignment. In the same diffractogram, the peak present at 69.11 degrees remained unassigned. The diffractogram of *Sample B* presents peaks specific to alpha-brass (ICDD PDF Card No. 00-050-1333): peaks no. 11(42.37 degrees), 15 (49.21 degrees) and 21 (72.31 degrees) correspond to (111), (200) and (220) diffraction planes.
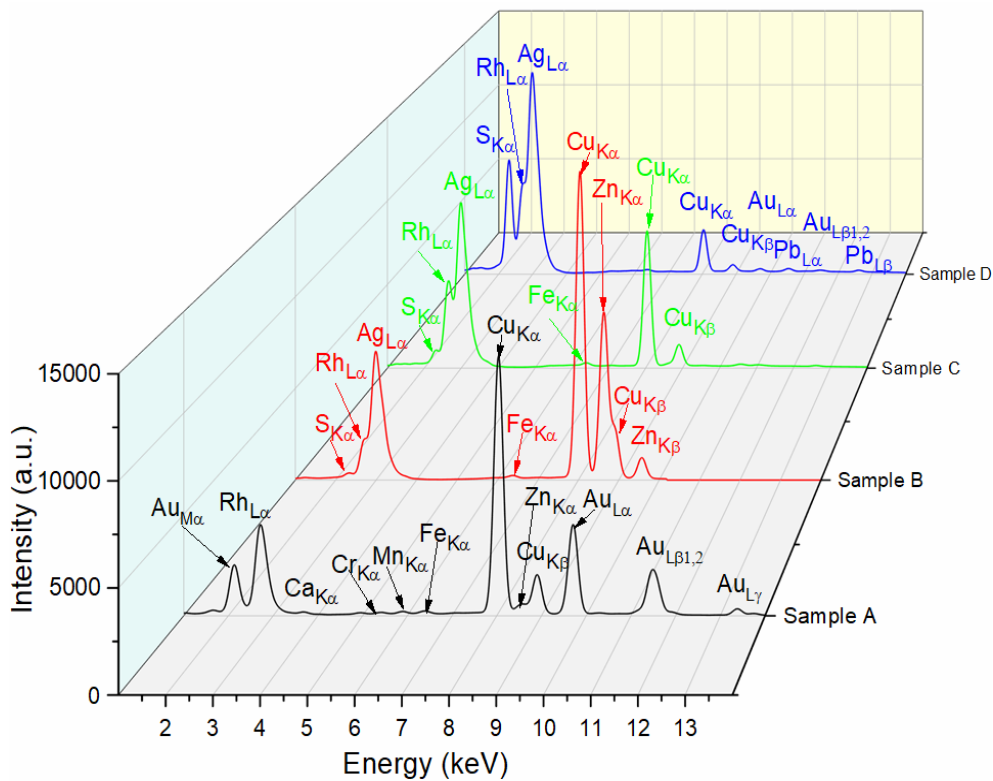

Fig. 3 – *Bulk* XRF spectra obtained for the analyzed samples.

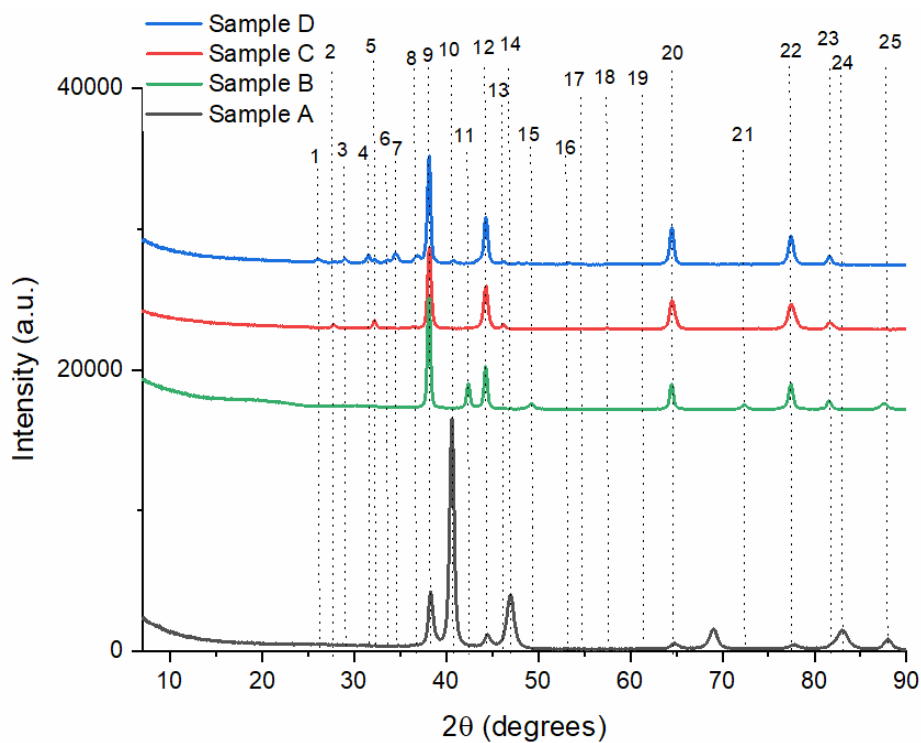| Sample	Element (%)								
	Al	S	Au	Ca	Mn	Fe	Cu	Zn	Ag
Sample A	0.6 ± 0.01	–	59.1 ± 0.3	0.83 ± 0.13	0.28 ± 0.01	0.37 ± 0.01	31 ± 0.4	0.68 ± 0.01	–
Sample B	–	1.36 ± 0.01	–	0.31 ± 0.07	0.008 ± 0.001	0.29 ± 0.01	24.3 ± 0.3	14.9 ± 0.4	57.2 ± 0.2
Sample C	0.5 ± 0.02	0.29 ± 0.05	–	0.6 ± 0.11	–	0.14 ± 0.01	11.9 ± 0.1	0.12 ± 0.02	77.46 ± 0.3
Sample D	0.1 ± 0.01	10.1 ± 0.4	0.18 ± 0.01	–	–	0.11 ± 0.01	2.8 ± 0.05	–	74.7 ± 0.2

Fig. 4 – *Bulk* XRD diffractograms obtained for the analyzed samples.

Sample C presents as major corrosion product Chlorargyrite, (ICDD PDF Card No. 00-031-1238) as demonstrated by peaks no. 2 (27.82 degrees), 5 (32.19 degrees), 13 (46.16 degrees), 17 (54.84 degrees) and 18 (57.38 degrees) corresponding to the

(111), (200), (220), (311) and (222) diffraction planes. Peaks no. 8 and 19 (at 36.38 and 61.28 degrees) correspond to the diffraction planes (111) and (220) of Cuprite (ICDD PDF Card No. 01-075-4299). Besides the peaks identified for Sample C, *Sample D* presents some peaks specific to another silver corrosion product (Acanthite – ICDD PDF Card No. 00-009-0422): 1 (26.04 degrees – (002) plane), 3 (28.99 degrees – (021) plane), 4 (31.53 degrees – (–311) plane), 6 (33.61 degrees – (121) plane), 7 (34.48 degrees – (220) plane) and 16 (53.38 degrees – (004) plane).

The *small area* analyses (PIXE and *micro-area* XRF) were aimed at obtaining a clearer image of the corrosion products and their distribution, by analyzing different points on the surface of the samples. The results are presented in Table 2, while the *micro-area* XRF spectra are presented in Fig. 5.

Table 2

Micro-area results (XRF and PIXE) obtained for the analyzed coins; N.D. – not detected. XRF 1 to 4 – the results obtained in the four analyzed points

Sample	Element (%)				
	Fe	Cu	Zn	Ag	Au
S.A XRF-1	N.D.	31.14 ± 0.05	0.64 ± 0.01	7.63 ± 0.02	60.53 ± 0.05
S.A XRF-2	N.D.	31.20 ± 0.06	0.70 ± 0.01	7.59 ± 0.03	60.14 ± 0.07
S.A XRF-3	N.D.	31.19 ± 0.05	0.65 ± 0.01	7.66 ± 0.02	60.49 ± 0.06
S.A XRF-4	N.D.	31.31 ± 0.05	0.64 ± 0.01	7.63 ± 0.03	60.36 ± 0.06
S.A PIXE	0.1 ± 0.02	20.6 ± 0.25	0.3 ± 0.06	5.8 ± 0.27	57.8 ± 1.09
S.B XRF-1	0.03 ± 0.004	53.94 ± 0.04	29.18 ± 0.04	16.55 ± 0.04	N.D.
S.B XRF-2	0.02 ± 0.004	53.82 ± 0.04	29.15 ± 0.04	16.74 ± 0.03	N.D.
S.B XRF-3	0.04 ± 0.005	51.58 ± 0.04	28.14 ± 0.05	19.98 ± 0.04	N.D.
S.B XRF-4	0.05 ± 0.005	52.68 ± 0.05	26.30 ± 0.05	20.82 ± 0.04	N.D.
S.B PIXE	0.1 ± 0.01	15.1 ± 0.17	3.3 ± 0.31	66.42 ± 3.38	N.D.
S.C XRF-1	N.D.	11.55 ± 0.03	0.05 ± 0.005	87.69 ± 0.04	0.20 ± 0.006
S.C XRF-2	0.17 ± 0.01	10.63 ± 0.04	0.45 ± 0.008	88.07 ± 0.04	0.22 ± 0.007
S.C XRF-3	0.45 ± 0.02	11.01 ± 0.04	0.14 ± 0.006	87.08 ± 0.05	0.79 ± 0.011
S.C XRF-4	N.D.	11.94 ± 0.04	0.29 ± 0.007	86.39 ± 0.04	0.88 ± 0.010
S.C PIXE	N.D.	4.6 ± 0.11	N.D.	86.8 ± 4.17	N.D.
S.D XRF-1	N.D.	2.55 ± 0.02	0.02 ± 0.002	96.33 ± 0.02	0.46 ± 0.007
S.D XRF-2	N.D.	2.89 ± 0.02	0.02 ± 0.003	95.76 ± 0.02	0.47 ± 0.008
S.D XRF-3	N.D.	3.19 ± 0.02	0.34 ± 0.006	95.12 ± 0.03	0.49 ± 0.007
S.D XRF-4	N.D.	2.62 ± 0.02	0.03 ± 0.003	96.01 ± 0.02	0.50 ± 0.008
S.D PIXE	N.D.	1.1 ± 0.06	N.D.	84.2 ± 3.80	N.D.

Besides the elements presented in Table 2, other elements were identified by *micro-area* XRF (*sample A* – Pb, point 1 – 0.056 ± 0.005, point 2 – 0.083 ± 0.006, point 4 – 0.055 ± 0.006; *Sample B* – Ni, point 1 – 0.112 ± 0.003, point 2 – 0.110 ± 0.003, point 3 – 0.106 ± 0.003, Pb, point 1 – 0.035 ± 0.003, point 2 – 0.033 ± 0.003, point 3 – 0.038 ± 0.003, point 4 – 0.042 ± 0.004; *Sample C* – Pb, point 1 – 0.499 ± 0.007, point 2 – 0.451 ± 0.007, point 3 – 0.522 ± 0.008, point 4 – 0.491 ± 0.007; *Sample D* – Pb, point 1 – 0.633 ± 0.007, point 2 – 0.857 ± 0.008, point 3 – 0.849 ± 0.008, point 4 – 0.851 ± 0.008), while by PIXE were identified Cl (0.3 ± 0.04 in Sample A, 0.1 ± 0.02 in Sample B, 0.8 ± 0.03 in Sample C, 0.1 ± 0.02 in Sample D), Ca (0.4 ± 0.04 in Sample A), Na (0.8% in Sample A, 0.5% in Sample B), Al (0.4 ± 0.06 in Sample A, 0.08 ± 0.02 in Sample C), Si (1.1 ± 0.07 in Sample A, 0.3 ± 0.022 in Sample B, 0.3 ± 0.02 in Sample C, 0.1 ± 0.01 in Sample D) and S (0.04% in Sample B and 3.3% in Sample D).
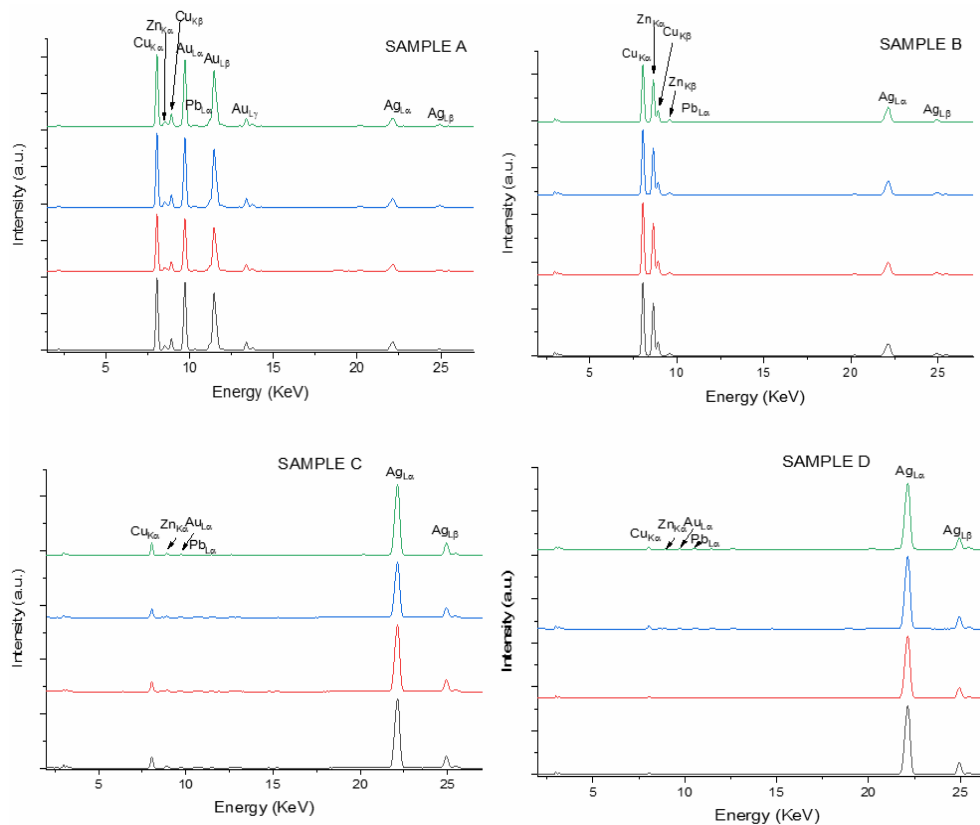

Fig. 5 – *Micro-area* XRF spectra obtained for the analyzed samples;
the analysis points are referred to as point 1 – the closest
to abscissa of the graph to point 4 – the farthest.

The *small-area* results are, generally, in good agreement with the *bulk* analyses. This is especially the case for Samples C and D, which, originating from coins have a relatively homogenous composition. The higher amount of silver found by *micro-area* XRF compared with PIXE can be explained by the phenomenon of apparent silver enrichment, as previously presented [9].

The differences in copper content could be explained by the presence on the surface of the samples of copper corrosion products. The results obtained for samples A and B suggest the presence of a deposition layer on the surface of the samples: if for Sample A, the results confirm the initial supposition of a gilded silver object, for Sample B, the results suggest a brass object covered with a silver layer. Also, the differences between *micro-area* XRF and PIXE could be explained by the differences in penetration depth of the two methods. If the conclusion regarding the composition of Sample A is heavily supported by the analytical data, a definitive conclusion regarding Sample B could not be drawn without the application of some destructive techniques; however, the application of such techniques is not desirable in the study of cultural heritage artifacts.

If the presence of lead in all samples can be easily explained by the technological processes the samples were subjected to, as other authors reported [23], the presence of nickel differentiate Sample B from the other analyzed samples, the element probably originating from the silver ores [9]. Also, the presence of trace amounts of zinc in samples A, C and D could be attributed to the silver source, while the high amount in Sample B supports the conclusion of a silver-plated brass object.

The other elements determined by PIXE (confirming the *bulk* XRF findings), can be divided in two categories: those originating from the corrosion products (such as chlorine or sulphur) and elements due to the external contamination of the samples (after the manufacturing process, for example during burial), such as sodium, aluminum, calcium and silicon [24].

Any discussion regarding the composition of the analyzed samples should take into consideration the different origin of the samples: if samples A and B are manufactured in the late XIXth-early XXth century, samples C and D are obtained from ancient coins. Thus, the presence of trace elements in samples C and D cannot lead to a definitive conclusion regarding the silver source, due to the very encountered recycling process [7]. This, in turn, leads to the presence of multiple trace elements, affecting the possibility of tracing different objects to original ores.

Another subject of interest regarding the analysis of the samples was represented by the interventions made on the ancient coins to be transformed into finery. Supplementary *micro-area* XRF analyses were performed in order to evaluate the interventions (results presented in Fig. 6) – disc, pin and rings on

Sample C, respectively the joint area, where a needle was welded onto the coin, in order to transform it into a brooch.

The results of the analyses show a composition of the selected areas different than the ones of the objects (Table 3). Thus, for Sample C it can be observed an increase of Co and Zn and a decrease of the silver content. However, the most spectacular change is represented by the variation of the gold content, leading to the conclusion that the pins/rings are made of a gold alloy. Sample D also presents a decrease in silver content, together with an approx. 4 times increase of Co and Zn content. This in turn suggests that the welding was performed using as material either brass or a silver/copper/zinc alloy, not pure silver.
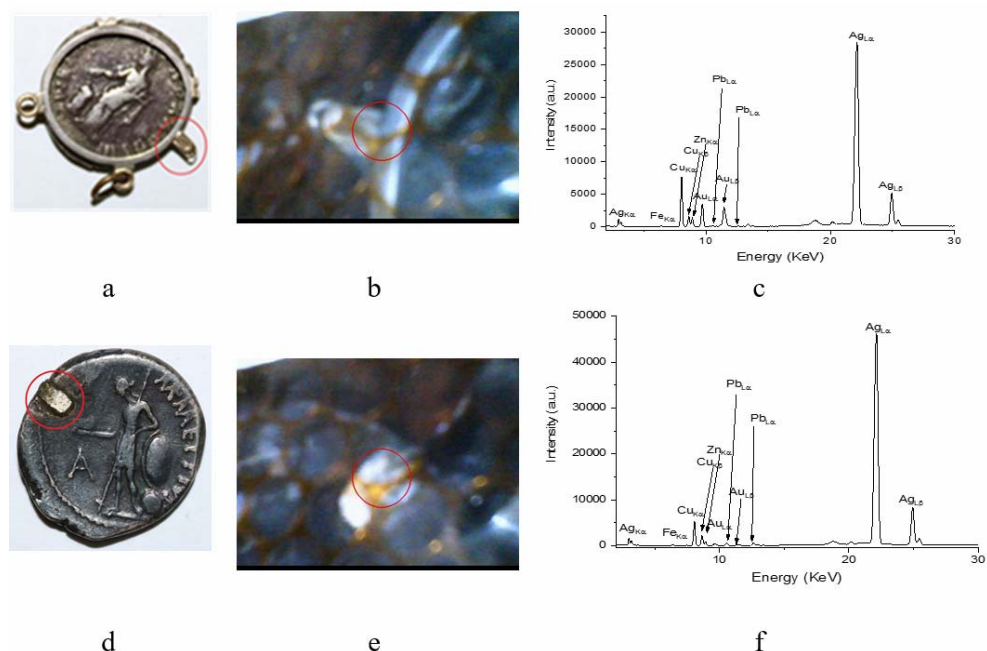

Fig. 6 – *Micro-area* XRF analysis of selected areas: a, d – identification of the areas;
b, e – images of the analyzed areas obtained with the spectrometer's camera;
c, f – obtained spectra; a, b, c – sample C; d, e, f – sample D.

Table 3

Micro-area XRF analysis of the selected areas; N.D. – not detected

Analyzed area	Element (%)						
	Pb	Au	Co	Fe	Cu	Zn	Ag
1 (Fig. 6c)	0.29 ± 0.008	7.78 ± 0.04	0.04 ± 0.009	0.72 ± 0.02	15.56 ± 0.06	2.04 ± 0.02	73.56 ± 0.07
2 (Fig. 6f)	0.69 ± 0.009	0.41 ± 0.009	N.D.	0.91 ± 0.02	8.19 ± 0.04	2.19 ± 0.02	87.58 ± 0.05

The *small-area* XRD results, presented in Fig. 7, offer supplementary information regarding the corrosion products and their distribution on the surface of the samples.
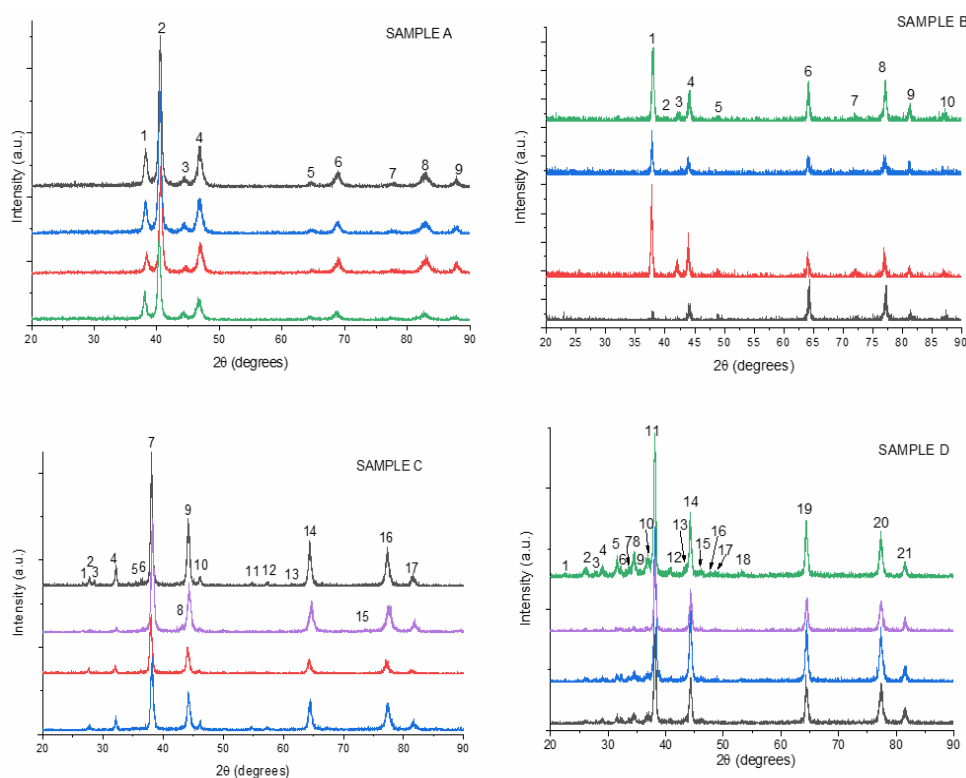

Fig. 7 – *Small-area* XRD diffractograms obtained for the analyzed samples;
the analysis points are referred to as point 1 – the closest
to abscissa of the graph to point 4 – the farthest.

The assignment of the identified peaks for the *small-area* diffractograms is presented in Table 4.

The identification of the compounds presented in Table 4 was made by comparison with the entries in ICDD Database: Silver-copper alloy (ICDD PDF Card No. 04-010-7444), Silver-Zinc alloy (ICDD PDF Card No. 00-029-1155), Zincite (ICDD PDF Card No. 00-036-1451), Gold (ICDD PDF Card No. 00-001-1172), alpha-brass (ICDD PDF Card No. 00-050-1333), Paratacamite (ICDD PDF Card No. 01-070-0821), Chlorargyrite (ICDD PDF Card No. 00-031-1238), Cuprite (ICDD PDF Card No. 01-075-4299), Tenorite (ICDD PDF Card No. 00-002-1040), Acanthite (ICDD PDF Card No. 00-009-0422).

Table 4

Assignment of the diffraction peaks from the *small-area* XRD analyses.

Peak No. in Fig. 7	SAMPLE A		SAMPLE B		SAMPLE C		SAMPLE D	
	Degrees (2θ)	Assignment	Degrees (2θ)	Assignment	Degrees (2θ)	Assignment	Degrees (2θ)	Assignment
1	38.16	(111) Silver copper	38.15	(111) Silver copper	26.35	(220) Paratacamite	22.36	(300) Paratacamite
2	40.69	(110) Silver Zinc	39.99	(110) Silver Zinc	27.81	(111) Chlorargyrite	25.92	(002) Acanthite
3	44.21	(200) Silver copper	42.12	(111) Brass	29.11	(110) Cuprite	27.74	(111) Chlorargyrite
4	47.21	(102) Zincite	44.18	(200) Silver copper	32.19	(200) Chlorargyrite	28.92	(021) Acanthite
5	64.35	(220) Silver copper	49.16	(200) Brass	35.52	(002) Tenorite	31.52	(−311) Acanthite
6	69.10	Unassigned	64.30	(220) Silver copper	36.35	(111) Cuprite	32.16	(200) Chlorargyrite
7	77.40	(311) Silver copper	72.09	(220) Brass	38.11	(111) Silver copper	33.57	(121) Acanthite
8	82.36	(222) Gold	77.23	(311) Silver copper	42.82	(200) Cuprite	34.52	(220) Acanthite
9	87.88	(220) Silver Zinc	81.23	(222) Silver copper	44.11	(200) Silver copper	35.47	(002) Tenorite
10			87.33	(311) Brass	46.23	(220) Chlorargyrite	36.72	(111) Cuprite
11					54.64	(311) Chlorargyrite	38.15	(111) Silver copper
12					57.35	(222) Chlorargyrite	40.67	(130) Acanthite
13					61.32	(220) Cuprite	43.43	(−123) Acanthite
14					64.51	(220) Silver copper	44.30	(200) Silver copper
15					73.46	(311) Cuprite	46.14	(220) Chlorargyrite
16					77.24	(311) Silver copper	47.61	(027) Paratacamite
17					81.61	(222) Silver copper	48.56	(−202) Tenorite
18							53.29	(004) Acanthite
19							64.33	(220) Silver copper
20							77.30	(311) Silver copper
21							81.55	(222) Silver copper

The *small-area* diffractograms of sample A are very similar with the *bulk* diffractograms, without any new peak's appearance; also, no intensity variation was observed. This leads to the conclusion that the sample has a very uniform surface composition, without any corrosion points. Sample B presents variation of the intensity of some of the diffraction peaks: 1, 4, 6, 8 (offering information related to several characteristics, such as grain size or residual stress, as previously presented by our group [9]); in the same time, other peaks are appearing only in some of the analyzed points: peak 2 in points 3 and 4, peak 3 in points 2 and 4, peak 5 in points 1, 2 and 4, peak 10 in points 1, 2 and 4. Diffractograms of Sample C maintains the same relative intensity of the major peaks. However, the *small-area* diffractograms evidenced the presence of another two corrosion products (paratacamite and tenorite), not determined by *bulk* analysis (both compounds only visible in point 4). In the same time, other peaks are appearing in only some of the analyzed points: peaks 3, 5, 6 and 13 in point 4, peaks 8 and 15 in point 3, peaks 11 and 12 in points 1 and 4. The analysis of Sample D confirms the fact that it is most affected by corrosion. Several corrosion products are present, both from silver and copper corrosion phenomenon. Supplementary to the information obtained from the *bulk* analysis there can be identified two more corrosion products: tenorite and paratacamite, both more visible in points 1, 2 and 4. Point 4 presents the most diffraction peaks, while point 3 presents the least peaks from the analyzed points. It must be stated that the analysis summarized in Table 4 presents *the most probable* corrosion compounds, as several of the peaks could be assigned to more than one corrosion products (as we previously presented [9]; this is also the case of gold/silver-copper alloy overlap, as previously discussed for the *bulk* analysis). The presence of multiple copper corrosion products on the surface of samples C and D confirms the supposition made on the discussions regarding the *micro-area* elemental analyses.

4. CONCLUSIONS

By the combined use of different techniques (optical microscopy, *bulk* and *small-area* XRD, *bulk* and *micro-area* XRF, PIXE), several finery objects were characterized, thus obtaining information that could not be obtained from their individual use. From the four analyzed objects, two were proven to be constructed using the coating technique: sample A consisted of gilded silver, while sample B most probably of silver-plated brass. A definitive conclusion regarding sample B cannot be drawn without performing destructive analysis. Samples C and D were obtained by welding different accessories to ancient coins. The welding points also offered interesting observations regarding the composition of the accessories.

REFERENCES

1. I. Crina Anca Sandu, M. Helena de Sá and M. Costa Pereira, Surf. Interface Anal. **43**, 1134–1151, DOI:10.1002/sia.3740, (2011).
2. E. Kenny and E. Gackstetter Nichols, *Beauty around the World: A Cultural Encyclopedia*, ABC-CLIO, LLC, USA, 2017.
3. M. F. Guerra, X-ray Spectrom. **37**(4), 317–327 (2008), DOI:10.1002/xrs.1013
4. P. Craddock, *Historical survey of gold refining. Part 1 and 2,* In: A. Ramage and P. T. Cradock (Eds.) *Kings Croesus' Gold; Excavations at Sardis and the History of Gold Refining*, British Museum Pubns Ltd, London, 2000, pp. 27–71.
5. N. Thomas, Hypothèses **1**(9), 175–186 (2006); DOI : 10.3917/hyp.051.0175.
6. J. Novakovic, P. Vassiliou and E. Georgiza, Int. J. Electrochem. Sci. **8**, 7223 – 7232 (2013).
7. R.C. Fierascu, I. Fierascu, A. Ortan, C. Constantin, D.A. Mirea and M. Statescu, Nucl. Instrum. Methods Phys. Res. B **401**, 18–24 (2017).
8. M. Watanabe, S. Shinozaki, E. Toyoda, K. Asakura, T. Ichino, N. Kuwaki, Y. Higashi and T. Tanaka, Corrosion **62**(3), 243–250 (2006); DOI: 10.5006/1.3278270.
9. I. Fierascu, R.C. Fierascu, A. Ortan, D.A. Mirea and C. Morarescu, Rom. Rep. Phys. **70**(4), 802 (2018).
10. D. Cristea-Stan, B. Constantinescu, G. Talmatchi and D. Ceccato, Rom. Journ. Phys. **61**(3–4), 445–456 (2016).
11. R. Radvan, C. Bors and L. Ghervase, Rom. Journ. Phys. **61**(9–10), 1530–1538 (2016).
12. B. Constantinescu, D. Cristea-Stan, D. Ceccato and C. Luculescu, Proc. Romanian Acad. A **18**(4), 308–314 (2017).
13. I. Dumitriu, R.C. Fierascu, A. Catangiu, M. Neata, R.M. Ion and R. Somoghi, J. Optoel. Adv. Mat. **13**, 874–878 (2011).
14. R.C. Fierascu, R.M. Ion and I. Fierascu, Instrument. Sci. Technol. **43**, 107–114 (2015);
15. A. Vasilescu, B. Constantinescu, D. Stan, G. Talmatchi and D. Ceccato, Nucl. Instrum. Methods Phys. Res. B **406**, 302–308 (2017).
16. S. Serafima, O.G. Duliu, M.M. Manea, A.V. Bojar, C. Costea, D. Birgaoanu and O.C. Barbu, Rom. Rep. Phys. **71**, 201 (2019).
17. I. Burducea, M. Straticiuc, D.G. Ghita, D.V. Mosu, C.I. Calinescu, N.C. Podaru, D. Mous, I. Ursu and N.V. Zamfir, Nucl. Instrum. Methods Phys. Res. B **359**, 12–19 (2015).
18. J.A. Maxwell, J.L. Campbell and W.J. Teesdale, Nucl. Instrum. Methods Phys. Res. B **43**, 218–230 (1989).
19. B. Constantinescu, D. Cristea-Stan, Z. Szőkefalvi-Nagy, I. Kovács, I. Harsányi and Z. Kasztovszky, Nucl. Instrum. Methods Phys. Res. B **417**, 105–109 (2018).
20. R. Bugoi, C. Talmaţchi, C. Haită and D. Ceccato, Nucl. Instrum. Methods Phys. Res. B **417**, 110–114 (2018).
21. J.C. D'Ars de Figueiredo, S.S. Asevedo and J.H.R. Barbosa, Appl. Surf. Sci. **317**, 67–72 (2014).
22. O. Abdel-Kareem, A. Al-Zahrani and M. Arbach, J. Archaeol. Sci. Rep. **9**, 565–576 (2016).
23. A. Vasilescu, B. Constantinescu, D. Stan, M. Radtke, U. Reinholz, G. Buzanich and D. Ceccato, Radiat. Phys. Chem. **117**, 26–34 (2015).
24. G.M. Ingo, C. Riccucci, M. Pascucci, E. Messina, C. Giuliani, G. Fierro and G. Di Carlo, Appl. Surf. Sci. **446**, 279–286 (2018).